


Supersoft elasticity and slow dynamics of isotropic-genesis polydomain liquid crystal elastomers investigated by loading- and strain-rate-controlled tests

Asaka Takebe and Kenji Urayama *Department of Macromolecular Science and Engineering, Kyoto Institute of Technology, Matsugasaki, Sakyo-ku, Kyoto 606-8585, Japan* (Received 18 May 2020; accepted 25 June 2020; published 13 July 2020)

The supersoft elasticity and slow dynamics of isotropic-genesis polydomain nematic elastomers are investigated by loading- and strain-rate-controlled tests. Loading-controlled tests reveal the stretching-driven polydomain-to-monodomain (PM) transition under true equilibrium condition without viscoelastic (time) effect. The equilibrium PM transition is observed as a discontinuous dimensional change at a threshold stress with extremely small magnitude ($\sigma_{PM}^{\infty} \approx 1$ kPa). The mechanical work required for 80% elongation of the elastomer accompanying the PM transition is only 2% of that required in the high-temperature isotropic state, reflecting the supersoft elasticity effect. The dimensional growth rate (R) under constant loading becomes low as the imposed stress (σ_0) approaches σ_{PM}^{∞} . The dependency of the dimension on the reduced time (Rt) is, however, independent of σ_0 . In the strain-rate ($\dot{\epsilon}$) controlled tests, the stress-stretch curves show a plateau region characteristic of the PM transition in a finite range of stretch, which is equivalent to the discontinuous stretch in the loading-controlled tests. The plateau stress σ_{pl} significantly decreases with decreasing $\dot{\epsilon}$, whereas the σ_{pl} at the practically accessible low strain rate (on the order of 10^{-4} s^{-1}) is still significantly higher than σ_{PM}^{∞} . The dependency of σ_{pl} on $\dot{\epsilon}$ is almost similar to the dependency of σ_0 on R in the loading-controlled tests. This similarity signifies that the two types of tests with different controlled stimuli are governed by the same dynamics of the local director.

DOI: [10.1103/PhysRevE.102.012701](https://doi.org/10.1103/PhysRevE.102.012701)

I. INTRODUCTION

Liquid crystal elastomers (LCEs) exhibit unique physical properties that result from the combination of rubber elasticity and liquid crystal (LC) orientation [1,2]. Owing to the strong correlation between the macroscopic shape and the LC orientation, LCEs deform with a change in temperature, electric field, and light irradiation, each of which induces a change in LC alignment [3–5]. These actuation properties allow the application of LCEs to soft actuators. The coupling of LC alignment and rubber elasticity also results in interesting mechanical properties, which are often called “soft elasticity” [1]. Nematic elastomers (NEs) possess the Goldstone-like soft modes in which the elastomer is deformed from one ground state to another accompanying the director rotation [6,7]. NEs require considerably small forces for the stretching in a direction at a finite angle to the initial director, because the stretching is assisted by the spontaneous elongation induced by the director realignment. NEs also exhibit large dissipation of mechanical energy under oscillatory strains reflecting director dynamics [8–10].

NEs are classified into monodomain (MNEs) and polydomain NEs (PNEs), depending on the director configuration. MNEs possess a globally uniform director alignment, while PNEs have a randomly disordered director configuration. Uniaxial stretching of PNEs drives a transition to the monodomain state with the global director along the stretching axis. The soft elasticity effect in the stretching-

driven polydomain-to-monodomain (PM) transition emerges as a small constant force in a finite range of stretch [11–14]. The mechanical work for finite stretching of PNEs becomes considerably small when undergoing the PM transition via the local Goldstone-like modes. PNEs can be obtained via two different routes, i.e., by cross-linking in the low-temperature polydomain nematic state (nematic genesis), and in the high-temperature isotropic state (isotropic genesis). We experimentally revealed that the effect of soft elasticity is more pronounced in PNEs with isotropic genesis (I-PNEs) than in those with nematic genesis (N-PNEs) [15]. I-PNEs require considerably lower mechanical work for the PM transition, compared with N-PNEs [15,16]. This is in qualitative agreement with the simulation results of Uchida [17]. I-PNEs also show markedly larger electromechanical effects than N-PNEs [18]. I-PNEs have no inherent memory of the initial director configuration owing to the cross-linking in the randomly disordered isotropic state, thus enabling local directors to respond without appreciable restrictions to external stimuli. I-PNEs are also characterized by randomly aligned local domains with fine and uniform sizes [15,19]. The extremely soft mechanical response of I-PNEs is referred to as “supersoft elasticity” [20]. The supersoft elasticity was investigated theoretically [20,21], and studied through simulation [17,22]. They showed that the supersoft elasticity of I-PNEs results from the great freedom for local directors to rotate and slide.

Another important characteristic of I-PNEs is the extremely slow dynamics of the local director. The dynamics was observed both by a slow stress relaxation following an imposed step strain [23], and by slow shape recovery after the removal of the imposed field [24]. The stretching-driven

*urayama@kit.ac.jp

PM transition is a typical phenomenon that reflects soft elasticity, and it has been studied for various types of PNEs [11–13,15,16,25]. Most previous experiments were conducted using conventional tensile tests with a constant strain rate or crosshead speed. They showed that the plateau stress (σ_{pl}), which characterizes the mechanical work required for the PM transition (W_{PM}), significantly decreases with a reduction in strain rate [23,25]. This strong strain rate dependence of σ_{pl} indicates the slow dynamics of the local director and also the difficulty in obtaining the true equilibrium value of σ_{pl} (σ_{pl}^{∞}) without a time effect. In other words, conventional stretching tests with finite strain rate tend to yield larger values of σ_{pl} (or W_{PM}) than expected, because of the inclusion of the viscoelastic (time) effect.

The evaluation of σ_{pl}^{∞} is important for a full understanding of the supersoft elasticity of I-PNEs. The value of σ_{pl} for the real I-PNEs is extremely small but finite in contrast to the ideal soft elasticity concept expecting zero value for σ_{pl} [1,6,16]. A nonzero value of σ_{pl} for the real I-PNEs is attributed to the presence of cross-links and network defects. There is, however, no quantitative understanding of the magnitude of σ_{pl} , although a theoretical model considers the deviation from the ideality [20,21]. The characterization of the true equilibrium value of σ_{pl} provides an important basis to describe quantitatively the supersoft elasticity of the real I-PNEs.

A loading-controlled test is appropriate to evaluate the critical stress for the PM transition (σ_{PM}^{∞}) under a true equilibrium condition. In loading-controlled tests, the equilibrium elongation of the specimens is measured as a function of the imposed loading. To confirm the equilibrium at each loading, one has to wait for a sufficiently long time, which is time consuming but free from instrumental restrictions. The PM transition in the loading-controlled tests emerges as a discontinuous dimensional change at σ_{PM}^{∞} . Loading-controlled tests are also expected to contribute to elucidate the slow dynamics of I-PNEs through the time development of the dimension at each loading. Thus, although they have rarely been conducted, the loading-controlled tests are important to characterize the equilibrium and dynamic aspects of the PM transition. Some studies [11–13,26] in the early stage of PM transition investigations employed this method, but σ_{PM}^{∞} for I-PNE was not fully characterized and the dynamics of dimensional growth was not examined.

Here, we report the characterization of the PM transition of I-PNEs under true equilibrium conditions using loading-controlled tests. The slow dynamics of the PM transition is also discussed considering the time development of the longitudinal dimension under constant loading, and the strain rate dependence of the plateau stress, each of which is obtained by loading- and strain-rate-controlled tests, respectively. We show that these independent results are governed by the same dynamics of the local director in the PM transition.

II. METHODS

A. Sample preparation

A main-chain polydomain nematic elastomer with isotropic genesis (I-MCPNE) was prepared using the method of Yakacki *et al.* [27]. The elastomer was made

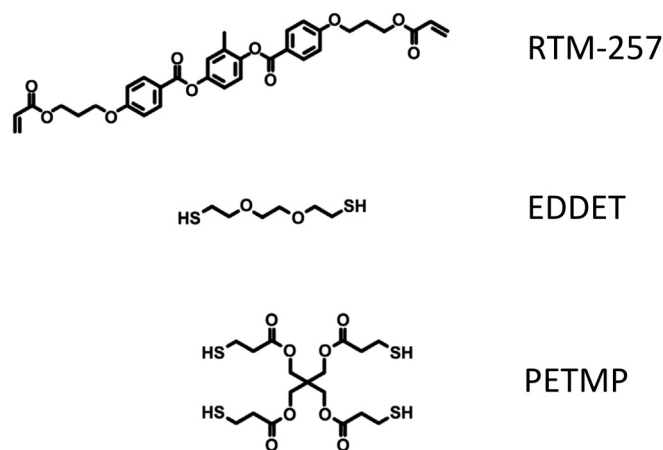


FIG. 1. Chemical structures of diacrylate mesogen, dithiol flexible spacer, and tetrathiol cross-linker.

by the Michael addition of dithiol flexible spacers (EDDET), tetrathiol cross-linkers (PETMP), and diacrylate mesogens (RTM-257). EDDT and PETMP were purchased from Sigma-Aldrich, and RTM-257 was obtained from Osaka Organic Chemical Industry. The chemical structures of these compounds are shown in Fig. 1.

These compounds were dissolved in toluene at 80 °C, and the concentration of the total compounds was 70 wt %. The molar ratio of RM-257/EDDET/PETMP was 1/0.74/0.06. The catalyst (dipropyl amine) solution was added to the mixture solution at 25 °C. The resulting solution was transferred to a mold and left to undergo gelation at 25 °C, where the mixture was in the isotropic state. The resultant freestanding gel film was transparent, ensuring cross-linking in the isotropic state, i.e., isotropic genesis. The gel was allowed to swell in toluene to remove the unreacted materials. The swollen gel was gradually deswollen by the stepwise addition of methanol (poor solvent) to toluene. The I-MCPNE film was obtained by drying the film under reduced pressure at 80 °C. The film had a turbid appearance characteristic of the polydomain texture.

B. Constant crosshead speed test

A uniaxial tensile test at a constant crosshead speed was conducted at 20 °C with a universal tester, AC-500N-CM (TSE, Japan). Specimens with dimensions of 30 × 6 × 1 mm or 5 × 1 × 1 mm were stretched with various constant crosshead speeds (8.3, 3.3, 0.33, and 0.0033 mm/s) to $\lambda = 2.5$ where λ is the stretch ratio given by the ratio of the dimensions in the deformed and undeformed states. The imposed maximum stretch ($\lambda = 2.5$) at each test was smaller than the fracture point to ensure that the same specimen could be used throughout the measurements for unambiguous comparison. The stretched specimen did not completely recover the initial dimension at 20 °C upon unloading. For the recovery to the initial dimensions, the unloaded specimen was placed on a hot stage for 2 min at 100 °C, which is beyond the nematic-isotropic transition point (ca. 80 °C), and then cooled to 20 °C. The specimen subjected to this heating treatment was used for the subsequent tensile tests, because the mechanical properties were reproducible.

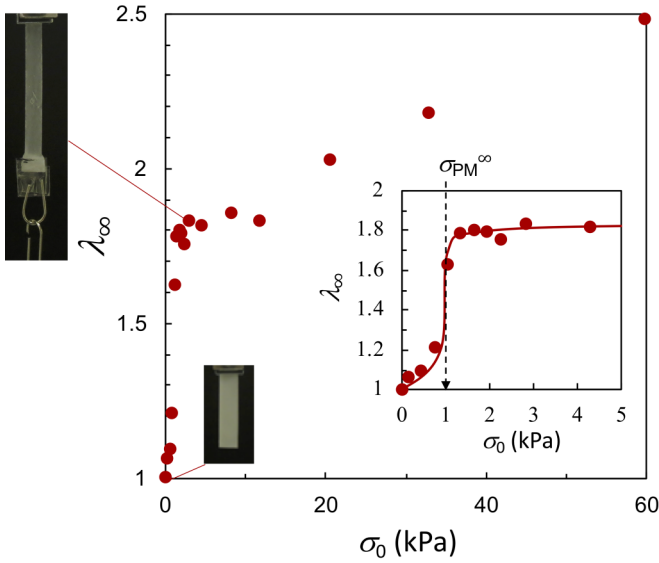


FIG. 2. Equilibrium elongation (λ_∞) as a function of imposed constant nominal stress (σ_0) obtained by the loading-controlled experiments. Inset shows the magnification of the small σ_0 region. A discontinuous dimensional change is an indication of the PM transition, and the equilibrium threshold stress for the transition (σ_{PM}^∞) is evaluated to be 1.0 kPa. The photographs show the turbid and semitransparent appearances in the undeformed and loaded states at $\sigma_0 = 2.8$ kPa, respectively.

C. Constant loading test

The time course of the stretch under constant loading was observed at 20 °C. A weight was suspended at the end of a rectangular specimen with dimensions of 30 × 6 × 1 mm. The longitudinal dimension under constant loading was measured as a function of elapsed time (t) until elongation equilibrium was attained. The imposed nominal stress (σ_0) was changed by varying the weight. The equilibrium elongation ($l_\infty = L_\infty/L_0$ where L_∞ and L_0 are the equilibrium dimensions under constant loading and the initial dimension, respectively) was investigated as a function of σ_0 . The same specimen was employed for the measurements at various values of σ_0 by using the heat treatment described in the previous section.

III. RESULTS AND DISCUSSION

Figure 2 illustrates the equilibrium elongation (λ_∞) as a function of the imposed nominal stress (σ_0) obtained by the loading-controlled experiments. The equilibrium elongation varies discontinuously at $\sigma_{PM}^\infty = 1.0$ kPa, and tends to increase with σ_0 . The discontinuous dimensional increase is a result of the polydomain-to-monodomain (PM) transition. This is clear from the change in the initial turbid appearance of the polydomain texture compared with the transparent appearance of the monodomain texture at $\sigma_0 > \sigma_{PM}^\infty$. The value of σ_{PM}^∞ (=1.0 kPa) obtained here is considerably lower than the typical reported values of the plateau stress (σ_{pl}) on the order of 10 kPa obtained by strain-rate ($\dot{\epsilon}$) controlled tests for various types of PNE, while it is comparable to that (=1.8 kPa) for a side-chain type I-PNE with acrylate network backbone evaluated from a stepwise stretching test where the stress at

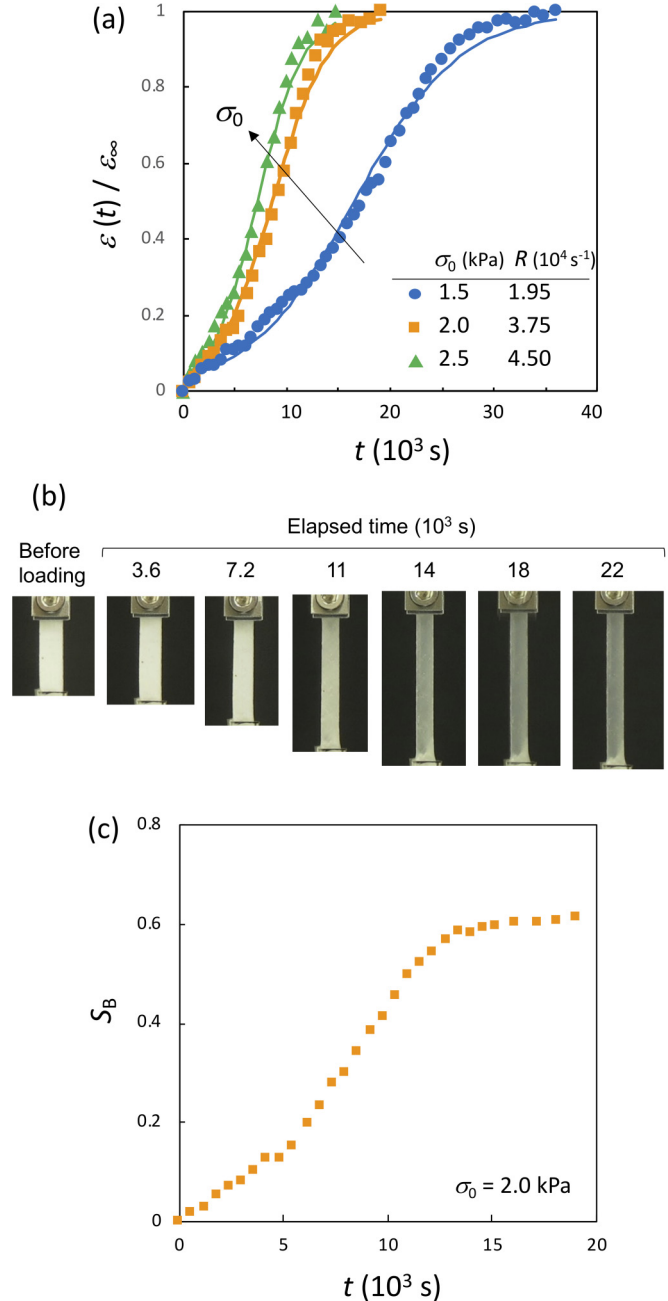


FIG. 3. (a) Time development of longitudinal strain $\epsilon(t)$ under various degrees of constant stress (σ_0). The strain is reduced by the equilibrium strain (ϵ_∞) at each loading. Solid lines represent the fitted curves of Eq. (2) with $c = 0.038$ using R as an adjustable parameter. (b) Appearance as a function of elapsed time after load imposition of $\sigma_0 = 2.0$ kPa. (c) Time development of the nematic order parameter for the network backbone (S_B) estimated from the data in (a) at $\sigma_0 = 2.0$ kPa with the anisotropic Gaussian network model.

each strain was equilibrated. [15] As demonstrated later, the strain rates employed in general strain-rate-controlled tests are so high that the viscoelastic (time) effect cannot be fully excluded for the I-PNEs. Clarke and Terentjev [23] estimated the equilibrium value of σ_{pl} by extrapolating the data at finite strain rates to zero strain rate. Their estimated value (about

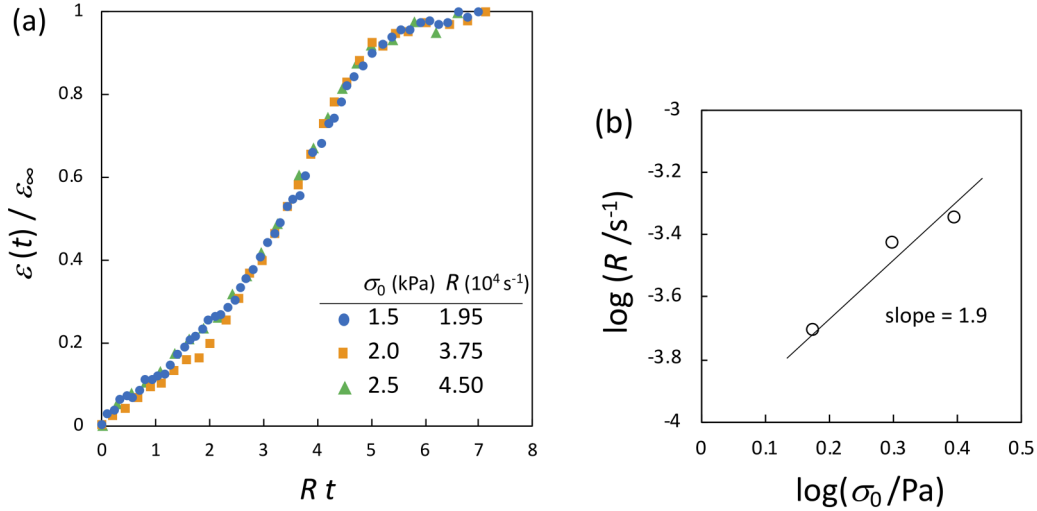


FIG. 4. (a) Reduced time course of $\varepsilon(t)/\varepsilon_\infty$ under various degrees of constant stress (σ_0). The elapsed time at each loading is reduced by the characteristic growth rate (R) obtained by the fitting of Eq. (2) to the $\varepsilon(t)$ - t data in Fig. 3(a). (b) Double logarithmic plots of R against σ_0 . The relation is approximated by $R \sim \sigma_0^{1.9}$. The base of the log in each axis is 10.

4 kPa) is close to but still larger than the value of $\sigma_{\text{PM}}^\infty$ obtained here.

In the σ_0 -controlled tests, when σ_0 is larger than but close to $\sigma_{\text{PM}}^\infty$, the PM transition is extremely slow. Figure 3(a) illustrates the time development of the nominal longitudinal strain ($\varepsilon = \lambda - 1$) under various degrees of σ_0 slightly larger than $\sigma_{\text{PM}}^\infty$. In the figure, $\varepsilon(t)$ is reduced by the equilibrium value ($\varepsilon_\infty = \lambda_\infty - 1$) at each σ_0 . The longitudinal dimension increases gradually with time and attains equilibrium at $t > 10^4$ s. Figure 3(b) shows the corresponding time development of the appearance. The specimen gradually elongates, accompanied with a change in the appearance from turbid to transparent due to an increase in nematic order along the loading direction. As can be seen in the figure, no appreciable (inhomogeneous) necking deformation was observed during the elongation process. The anisotropic Gaussian network model correlates the spontaneous elongation with the nematic order parameter of the network backbone (S_B) as [1]

$$S_B = \frac{\lambda^3 - 1}{\lambda^2 + 2}, \quad (1)$$

where S_B is zero in the undeformed and randomly disordered states ($\lambda = 1$ and $\varepsilon = 0$). Figure 3(c) displays S_B as a function of elapsed time calculated from the ε - t data at $\sigma_0 = 2$ kPa in Fig. 3(a). This loading finally causes a transition to the monodomain alignment with $\lambda_\infty = 1.8$ and $S_B \approx 0.6$.

The ε - t curves with sigmoidal shapes in Fig. 3(a) are fitted using a logistic growth function:

$$\frac{\varepsilon(t)}{\varepsilon_\infty} = \frac{1}{1 + (c^{-1} - 1)\exp(-Rt)}, \quad (2)$$

where R is the growth rate and c is the initial value at $t = 0$ [$c = \varepsilon(0)/\varepsilon_\infty$]. The solid curves in the figure represent the fitted curves using R as an adjustable parameter. The parameter R corresponds to the characteristic growth rate, and the value of R at each σ_0 is listed in the figure. From Fig. 3(a), it can be seen that the equilibration time becomes longer as σ_0 approaches $\sigma_{\text{PM}}^\infty$. Figure 4(a) compares the time courses of ε at

various degrees of σ_0 , where t is reduced by R at each σ_0 . The reduced curves at various σ_0 are almost collapsed into a single curve, indicating that the transition kinetics near the threshold is independent of σ_0 , whereas R decreases with a reduction in σ_0 . Figure 4(b) shows the double logarithmic plots of R against σ_0 . The relation is approximated by $R \sim \sigma_0^{1.9}$. This relation will be discussed later together with the results in the strain-rate-controlled tests.

Figure 5 shows the nominal stress (σ)-stretch (λ) relations of the I-MCPNE at various nominal strain rates ($\dot{\varepsilon}$) in the nematic and isotropic states. The nominal strain rate ($\dot{\varepsilon}$) is given by $\dot{\varepsilon} = V/L_0$, where V and L_0 are the crosshead speed and initial length, respectively. The σ - λ curves in the nematic state at $\dot{\varepsilon} \leq 0.41 \text{ s}^{-1}$ are characterized by an initial growth in stress followed by a plateau and a subsequent stress increase, as observed in previous studies for various polydomain nematic elastomers [11–13,15,16,25]. The plateau feature in a wide strain range is an indication of the PM transition. The σ - λ curves in the nematic state are considerably dependent on $\dot{\varepsilon}$. The stress σ increases with $\dot{\varepsilon}$, compared at the same λ . In contrast, the curves in the high-temperature isotropic state are independent of $\dot{\varepsilon}$, indicating that the pronounced effect of $\dot{\varepsilon}$ on σ in the nematic state originates from the dynamics of the local director, not from the viscoelasticity of the nonuniform polymer network structure. The PM transition is characterized by a change in the appearance from turbid to transparent in addition to the plateau feature. In the high-speed stretching of $\dot{\varepsilon} = 1.6 \text{ s}^{-1}$, however, the specimen remained considerably turbid even at high λ (Fig. 5), and σ increased with λ showing no definite plateau. These features at $\dot{\varepsilon} = 1.6 \text{ s}^{-1}$ indicate that the corresponding strain rate is so high that the director realignment cannot follow the imposed strain, resulting in no definite PM transition.

The stretch ($\lambda_\infty \approx 1.8$) in the onset of the monodomain regime in the σ_0 -controlled test (Fig. 2) was similar to that at the end of the quasiplateau region in the $\dot{\varepsilon}$ -controlled tests. Figure 5(b) compares the σ - λ data obtained at the slowest strain rate ($\dot{\varepsilon} = 0.00016 \text{ s}^{-1}$) with the σ_0 - λ_∞ data in the

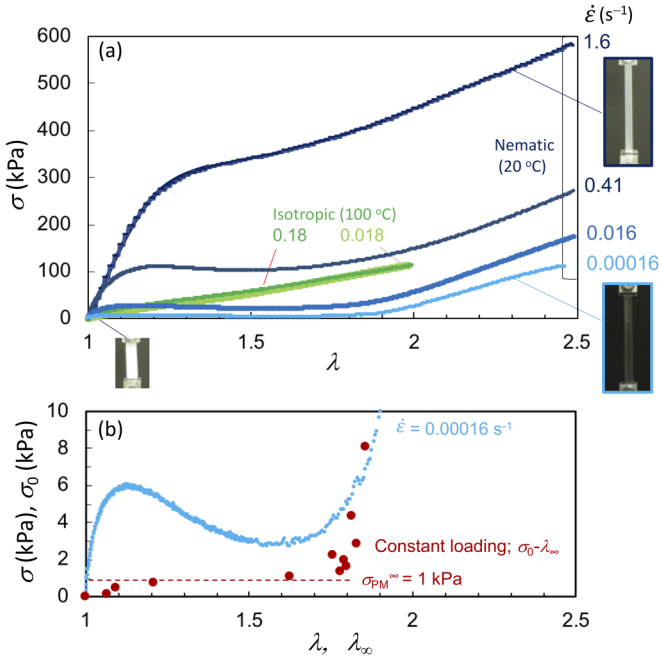


FIG. 5. (a) Nominal stress (σ)–elongation (λ) relations at various nominal strain rates ($\dot{\epsilon}$) in the nematic and isotropic states. The transparent appearance at $\lambda = 2.3$ in the stretching of $\dot{\epsilon} = 0.00016 \text{ s}^{-1}$ shows the monodomain alignment. The appearance at $\lambda = 2.3$ in the high-speed stretching of $\dot{\epsilon} = 1.6$ remains turbid, indicating that definite PM transition does not occur. (b) Comparison of the stress–stretch relation obtained by the $\dot{\epsilon}$ -controlled experiment of the slowest strain rate [0.00016 s^{-1} in (a)] with the equilibrium relation (Fig. 2) obtained by the σ_0 -controlled experiments.

loading-controlled tests (Fig. 2). Evidently, $\sigma_{\text{PM}}^{\infty}$ is significantly lower than σ at $\dot{\epsilon} = 0.00016 \text{ s}^{-1}$, indicating that the σ - λ relation is still far from the equilibrium even when $\dot{\epsilon}$ is considerably low (on the order of 10^{-4} s^{-1}). The undulation of the σ - λ curve at $\dot{\epsilon} = 0.00016 \text{ s}^{-1}$ is a result of finite stress relaxation during stretching. The equilibrium σ_0 - λ_{∞} relation also enables us to evaluate the mechanical work (W_{PM}^{∞}) without the time effect for the stretching of $\lambda = 1.8$, that is, the end of the plateau regime. The quantity W_{PM}^{∞} corresponds to the minimum mechanical work resulting from the soft elasticity effect, in which the elongation is induced by the director realignment. The estimated value of W_{PM}^{∞} (0.7 kJ/m^3) is only 2% of the corresponding mechanical work in the high-temperature isotropic state (40 kJ/m^3), which was estimated from the data in Fig. 5. The ideal soft elasticity concept expects zero mechanical work for elongation [1,6,17]. The presence of cross-links and network defects in real nematic elastomers, however, causes small but nonzero mechanical work in the transition from the initial polydomain states to the stretched monodomain states [20,21]. The true equilibrium behavior revealed here provides a basis to understand quantitatively the magnitude of the mechanical work required for the PM transition for the real I-PNEs.

Figure 6 shows the $\dot{\epsilon}$ dependence of the plateau stress (σ_{pl}) and stress in the monodomain state (σ_{pl}). The stresses σ_{pl} and σ_{pl} correspond to $\lambda = 1.5$ in the plateau region and $\lambda = 2.4$ in the post-transition region, respectively. The data points at

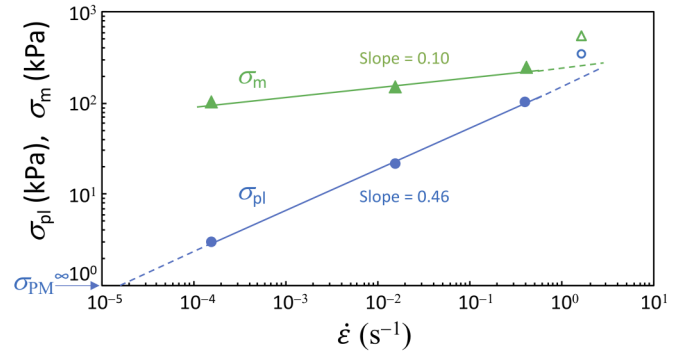


FIG. 6. Plateau stress (σ_{pl} at $\lambda = 1.5$) and stress in the monodomain state (σ_{pl} at $\lambda = 2.4$) as a function of the nominal strain rate ($\dot{\epsilon}$). The open symbols denote the data at high-speed stretching, which induces no definite PM transition. The strain rate required to equilibrate the stress during stretching was estimated to be $2 \times 10^{-5} \text{ s}^{-1}$ by extrapolating the power law behavior of $\sigma_{\text{pl}} \sim \dot{\epsilon}^{0.46}$ to the equilibrium value ($\sigma_{\text{PM}}^{\infty} = 1 \text{ kPa}$) obtained by the loading-controlled tests.

$\dot{\epsilon} \leq 0.41 \text{ s}^{-1}$ lie in a straight line; however, those at $\dot{\epsilon} = 1.6 \text{ s}^{-1}$ deviate from the correlations. As mentioned before, no definite PM transition occurs at $\dot{\epsilon} = 1.6 \text{ s}^{-1}$ due to the excessive strain rate, explaining the deviation from the dynamics of the PM transition. When undergoing the PM transition at $\dot{\epsilon} \leq 0.41 \text{ s}^{-1}$, σ_{pl} is significantly dependent on $\dot{\epsilon}$ ($\sigma_{\text{pl}} \sim \dot{\epsilon}^{0.46}$), whereas σ_{pl} is nearly independent of $\dot{\epsilon}$ ($\sigma_{\text{m}} \sim \dot{\epsilon}^{0.1}$), indicating that the dynamics in the transition and post-transition regimes are not identical. The pronounced $\dot{\epsilon}$ dependence of σ_{pl} reflects the dynamics of the director rotation. In contrast, almost no $\dot{\epsilon}$ dependence of σ_{pl} implies that the dynamics of the post-transition regime with monodomain alignment is governed by the low viscoelasticity of the rubbery polymer network structure.

The extrapolation of the σ_{pl} - $\dot{\epsilon}$ relationship in Fig. 6 to $\sigma_{\text{PM}}^{\infty}$ enables us to estimate the strain rate required to obtain the equilibrium value of $\sigma_{\text{pl}}^{\infty}$ ($\sigma_{\text{PM}}^{\infty} = 1 \text{ kPa}$) by the $\dot{\epsilon}$ -controlled tests. The estimated value of $\dot{\epsilon}$ is approximately $1.5 \times 10^{-5} \text{ s}^{-1}$, implying that the equilibration in the $\dot{\epsilon}$ -controlled tests requires an extremely slow elongation, more than 20 h, to stretch the present specimen to $\lambda = 2$.

The power law exponent for the σ_{pl} - $\dot{\epsilon}$ relation ($\sigma_{\text{pl}} \sim \dot{\epsilon}^{\beta}$; $\beta = 0.46$) (Fig. 6) is comparable to that for the relation $\sigma_0 \sim R^{\alpha}$ ($\alpha = 0.53$) obtained in the loading-controlled tests [$R \sim \sigma_0^{1.9}$ in Fig. 4(b)]. This similarity signifies that the same dynamics of the local director in the PM transition emerge in the two different types of tests with a reversal relation between the controlled stimulus and observed response.

We also show the response of the I-PNE upon unloading after the maximum stretch is imposed. Figure 7 illustrates the loading-unloading curve obtained at the slowest strain rate at $\dot{\epsilon} = 0.00016 \text{ s}^{-1}$. The unloaded specimen exhibits a residual stretch of $\lambda_{\text{R}} = 1.85$ which is close to the stretch at the end of the plateau regime. The residual stretch remained unchanged when left at $20 \text{ }^{\circ}\text{C}$ for 20 days, although the visual appearance gradually changed from transparent to slightly translucent, which is shown in the figure. The residual

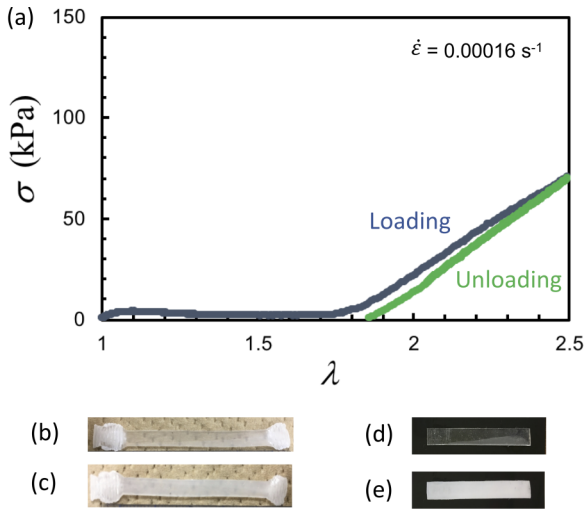


FIG. 7. (a) Nominal stress (σ)–elongation (λ) relations in the loading and unloading processes at the slowest strain rate of $\dot{\epsilon} = 0.00016 \text{ s}^{-1}$ at 20°C . (b) Immediately after unloading, the specimen exhibits a residual stretch of $\lambda = 1.85$ which is close to the stretch at the end of the plateau region. The portions at both ends correspond to the clamped parts in tensile tests. (c) The residual stretch for the unloaded specimen remains unchanged after 20 days at 20°C , while the visual appearance changes from transparent to slightly translucent, indicating a monodomain state with low orientational order near the PM transition threshold. (d) The unloaded specimen completely recovers the initial dimension after heating at 100°C beyond the nematic-isotropic transition temperature (about 80°C). (e) The turbid specimen with the initial dimension and polydomain texture is obtained by cooling at 20°C .

strain completely vanishes by the heating at 100°C beyond the nematic-isotropic transition temperature (about 80°C), and the specimen with the initial dimension and polydomain texture is obtained again by the subsequent cooling to 20°C . These behaviors suggest that the unloaded state with a residual stretch, i.e., a monodomain state with low orientational order near the transition threshold, corresponds to another ground state. This feature prevents the investigation of the monodomain-to-polydomain transition by the unloading process in the loading-controlled tests, although a discontinuous increase in length observed by the loading process (Fig. 2) is the hallmark of the instability of a subcritical or first-order

transition which is often accompanied by the finite hysteresis effect.

IV. SUMMARY

Loading-controlled tests revealed the PM transition of the nematic elastomers with isotropic genesis in the equilibrium condition, excluding the time effects. The mechanical work required for the stretching (ca. 80%) accompanying the PM transition (W_{PM}^∞) is only 2% of the mechanical work needed for the same degree of stretching in the high-temperature isotropic state. The extremely small degrees of mechanical work and threshold stress ($\sigma_{\text{PM}}^\infty = 1 \text{ kPa}$) originate purely from the soft elasticity effect, in which spontaneous elongation driven by the director realignment assists macroscopic elongation.

The dimensional growth during the PM transition in the σ_0 -controlled tests proceeds slowly when σ_0 is close to $\sigma_{\text{PM}}^\infty$. The dimensional growth rate (R) increases as σ_0 approaches $\sigma_{\text{PM}}^\infty$. However, the time course of the dimensional change is independent of σ_0 when the elapsed time is reduced by R at each σ_0 .

It is difficult to observe the equilibrium PM transition for the $\dot{\epsilon}$ -controlled tests because an unrealistically small magnitude of $\dot{\epsilon}$, on the order of 10^{-5} s^{-1} , is required. The characteristic plateau stress (σ_{pl}) in the transition regime significantly increases with $\dot{\epsilon}$, whereas the stress in the post-transition (monodomain) regime is almost independent of $\dot{\epsilon}$, indicating that these regimes obey different dynamics. The dynamics in the transition regime is governed by the slow dynamics of the local director, whereas that in the monodomain state indicates the modest viscoelasticity of the polymer network structure.

The dependence of σ_{pl} on $\dot{\epsilon}$ ($\sigma_{\text{pl}} \sim \dot{\epsilon}^{0.46}$) in the $\dot{\epsilon}$ -controlled tests is almost similar to the dependence of σ_0 on R ($\sigma_0 \sim R^{0.53}$) in the σ_0 -controlled tests. This similarity indicates that the same dynamics of the local director in the PM transition emerge in the two types of tests with a reversal relation between the controlled stimulus and observed response.

ACKNOWLEDGMENTS

This work is partly supported by JSPS KAKENHI Grant No. JP18H02034. The authors thank Osaka Organic Chemical Industry Ltd. for the provision of the diacrylate compound RM-257.

- [1] M. Warner and E. M. Terentjev, *Liquid Crystals Elastomers*, Revised Ed. (Clarendon Press, London, 2007).
- [2] K. Urayama, *Macromolecules* **40**, 2277 (2007).
- [3] T. J. White and D. J. Broer, *Nat. Mater.* **14**, 1087 (2015).
- [4] S. W. Ula, N. A. Traugott, R. H. Volpe, R. R. Patel, K. Yu, and C. M. Yakacki, *Liq. Cryst. Rev.* **6**, 78 (2018).
- [5] R. S. Kularatne, H. Kim, J. M. Boothby, and T. H. Ware, *J. Polym. Sci., Part B: Polym. Phys.* **55**, 395 (2017).
- [6] M. Warner, P. Bladon, and E. M. Terentjev, *J. Phys. II* **4**, 93 (1994).
- [7] L. Golubovic and T. C. Lubensky, *Phys. Rev. Lett.* **63**, 1082 (1989).
- [8] S. M. Clarke, A. R. Tajbakhsh, E. M. Terentjev, C. Remillat, G. R. Tomlinson, and J. R. House, *J. Appl. Phys.* **89**, 6530 (2001).
- [9] D. R. Merkel, R. K. Shaha, C. M. Yakacki, and C. P. Frick, *Polymer* **166**, 148 (2019).
- [10] P. Stein, N. Aßfalg, H. Finkelmann, and P. Martinoty, *Eur. Phys. J. E* **4**, 255 (2001).
- [11] J. Schatzle, W. Kaufhold, and H. Finkelmann, *Makromol. Chem.* **190**, 3269 (1989).
- [12] E. R. Zubarev, R. V. Talroze, T. I. Yuranova, N. A. Plate, and H. Finkelmann, *Macromolecules* **31**, 3566 (1998).

- [13] S. M. Clarke, E. M. Terentjev, I. Kundler, and H. Finkelmann, *Macromolecules* **31**, 4862 (1998).
- [14] S. V. Fridrikh and E. M. Terentjev, *Phys. Rev. E* **60**, 1847 (1999).
- [15] K. Urayama, E. Kohmon, M. Kojima, and T. Takigawa, *Macromolecules* **42**, 4084 (2009).
- [16] N. A. Traugott, R. H. Volpe, M. S. Bollinger, M. O. Saed, A. H. Torbati, K. Yu, N. Dadivanyan, and C. M. Yakacki, *Soft Matter* **13**, 7013 (2017).
- [17] N. Uchida, *Phys. Rev. E* **62**, 5119 (2000).
- [18] T. Okamoto, K. Urayama, and T. Takigawa, *Soft Matter* **7**, 10585 (2011).
- [19] H. Higaki, K. Urayama, and T. Takigawa, *Macromol. Chem. Phys.* **213**, 1907 (2012).
- [20] J. S. Biggins, M. Warner, and K. Bhattacharya, *Phys. Rev. Lett.* **103**, 037802 (2009).
- [21] J. S. Biggins, M. Warner, and K. Bhattacharya, *J. Mech. Phys. Solids* **60**, 573 (2012).
- [22] G. Skačej and C. Zannoni, *Macromolecules* **47**, 8824 (2014).
- [23] S. M. Clarke and E. M. Terentjev, *Phys. Rev. Lett.* **81**, 4436 (1998).
- [24] K. Urayama, S. Honda, and T. Takigawa, *Phys. Rev. E* **74**, 041709 (2006).
- [25] A. Azoug, V. Vasconcellos, J. Dooling, M. Saed, C. M. Yakacki, and T. D. Nguyen, *Polymer* **98**, 165 (2016).
- [26] K. Hammerschmidt and H. Finkelmann, *Makromol. Chem.* **190**, 1089 (1989).
- [27] C. M. Yakacki, M. Saed, D. P. Nair, T. Gong, S. M. Reed, and C. N. Bowman, *RSC Adv.* **5**, 18997 (2015).